

# Lithiumniobate Die Assembled by a Low-stress Soldering Technique

## Method to Fasten a Surface Acoustic Wave Sensor

Pol Ribes-Pleguezuelo<sup>1,2</sup>, Katherine Frei<sup>1</sup>, Gudrun Bruckner<sup>3</sup>, Erik Beckert<sup>1</sup>,  
Ramona Eberhardt<sup>1</sup> and Andreas Tünnermann<sup>1,2</sup>

<sup>1</sup>Fraunhofer Institute for Applied Optics and Precision Engineering IOF, Albert-Einstein-Str. 7, 07745 Jena, Germany

<sup>2</sup>Institute of Applied Physics IAP, Friedrich-Schiller University Jena, Max-Wien-Platz 1, 07743 Jena, Germany

<sup>3</sup>Carinthian Tech Research AG, Europastraße 12, A-9524, St. Magdalen, Austria

**Keywords:** Surface Acoustic Wave Sensor, Optical Crystal, Packaging, Solderjet Bumping Technique, Lithiumniobate.

**Abstract:** Solderjet bumping technique was applied to assemble a Surface Acoustic Wave (SAW) sensor prototype designed with a lithiumniobate crystal and a base sub-mount made of stainless steel. The assembly was designed with this technology in order to withstand the device's mechanical strength requirements. The initial performed tests showed that the solderjet bumping technique can be used to assemble brittle components without creating internal damage in the crystal. The selected solder alloy Au<sub>80</sub>Sn<sub>20</sub> used to fasten the lithiumniobate showed proper alloy wettability and joint strength on the crystal and on the substrate material. Finally, a lithiumniobate die device was soldered by soldering means to the stainless steel sub-mount, and withstood the strength device requirements by passing robustness (push) tests.

## 1 INTRODUCTION

### 1.1 Motivation

The demand from industry and consumer electronics for continuous miniaturisation and increased integration density of components can only be fulfilled by applying appropriate attachment and interconnection technologies. Smart systems require interconnection of heterogeneous materials like crystals, ceramics, printed circuit boards, screen printed layers, and metals. The die attachment processes are critical for the functionality of the devices. Depending on the application, the interconnection layer must act as a thermal or electrical contact, allowing power dissipation or compensating thermal mismatch of different materials.

Lithiumniobate (LN) is a material widely used in optics and as High Frequency (HF) filters. This piezo electric crystal is also used for Surface Acoustic Wave (SAW) based physical sensors, which work completely passively – without power supply, and can be interrogated wirelessly and used in temperature regions well above the operation range of silicon based devices (Reindl, 1998; Bruckner, 2017). The high temperature operation (300 °C) poses additional demands on the interconnection techniques.

In this work, we examine the solderjet bumping technique for the die attachment of LN chips to stainless steel, which promises several advantages when compared to common adhesives based on organic materials, as these materials are generally limited to temperatures below 280 °C. The final goal is to establish a bonding process that permits LN crystals to function as combined temperature and strain or pressure sensors in a wide temperature range (-100 °C to 300 °C) with high reproducibility and reliability.

SAW chips are commonly fixed using silicon based rather soft adhesives which allow low stress bonds, but are limited to ~ 200°C. During the last years we have tested high temperature stable epoxy- and polyimide based glues for the attachment of SAW dies in metallized and ceramic packages. All of these adhesives failed in long term tests where the samples were exposed to temperatures around 300°C for several months. We observed outgassing that resulted in contaminating layers on the SAW chips and disintegration on the adhesives. In extreme cases the glues disintegrated completely and the dies fell off. Any outgassing from the adhesives or package can raise chemical reaction in the microclimate of packaged devices which damage the delicate surface of SAW chips (Bardong 2016). Ceramic glues could be used, but the TCE mismatch often causes breaking

of the chips. Metal based attachment techniques are promising for high temperature and low stress die attachment (Roshanghias 2017) as they allow compensation of TCE mismatch and minimize mechanical stress. Solderjet bumping technique is especially suited, as no thermal stress is induced during the bonding process.

### 1.2 Solderjet Bumping Technique

Solder-joining using metallic solder alloys is an alternative to adhesive bonding. Laser-based soldering processes are especially well suited for the joining of optical components made of fragile and brittle materials such as glasses, ceramics and crystals, due to a localized and minimized input of thermal energy (Beckert, 2009).

Solderjet bumping (Figure 1) is a technique adapted from flip chip processing of semiconductor devices that also allows for the flux-free and contact-free processing of optical components and 3D-packaging. It uses spherical solder preforms of various soft solder alloys (e.g. tin-based lead-free solders, low melting indium alloys or high melting eutectic gold-tin, gold-silicon or gold-germanium solders) in a diameter range of 40 μm to 760 μm. The solder spheres are transferred from a reservoir to a placement capillary with a conical tip and an inner diameter that is slightly smaller than the diameter of the spheres. After positioning the capillary next to the joining geometry using an articulating robot, the solder alloy is molten by an infrared laser pulse and jetted out of the capillary by applying nitrogen pressure. The jetting of liquid solder volumes provides a very good thermal contact of the alloy with the components, and allows for the joining within complex 3D-integrated geometries. The bond head of the solderjet bumper integrates solder volume feeding, reflow, and application of liquid solder and allowing for highly automated and flexible use.

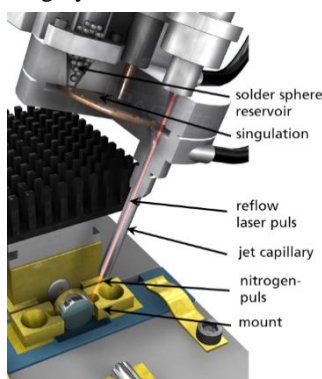


Figure 1: Schematic drawing of the solderjet bond head able to solder droplets with 6 degrees of freedom (DOF).

However, the formation of a metallic solder joint using components made of non-metallic materials with solderjet bumping requires a wettable metallization layer applied to the components. Such surfaces can be provided by thin film (e.g. physical vapour deposition) or thick film (e.g. screen printing of metal pastes) processes. Sputtered three-layer systems (Figure 2) using a titanium adhesion layer, a platinum diffusion barrier, and a noble gold finish preventing oxidization and acting as a wetting surface, provide superb conditions for wetting of liquid solder droplets (Banse, 2005).

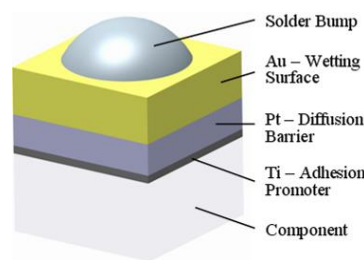


Figure 2: Example of three sputtered layers (Ti/Pt/Au) over the substrate component to later be able to create a wettable surface for the solder bump.

## 2 REQUIREMENTS

As stated before, the aimed operation temperature is 300 °C or higher while the processing temperature for LN is limited to about 450 °C for a short time. Die attachment by solderjet bumping with eutectic materials allows high temperature operation of the devices with minimum thermal stress induced during the attachment process. In addition, metals are ductile and can compensate thermal mismatch of different materials. This property is extremely important for LN, as the crystal is highly anisotropic. The thermal expansion coefficient in one direction is about three times bigger than in the other, preventing thermal matching to metal or ceramics. Furthermore, the metallic interface allows a good thermal contact between chip and support, which is crucial for the device to operate as temperature sensor.

For sensing of pressure or strain several geometries can be used. We have considered a cantilever setup, where the LN crystal is either mounted on a metallic cantilever beam, or forms the cantilever itself. In both configurations precise and reproducible mounting of the device with sufficient adhesion strength is essential. When solderjet bumping is used, the die can be put in direct contact with the metal of the pressure sensor. This is a big advantage compared to any attachment technique

using an interface layer, as any adhesive within the chip-metal interface would affect the device sensitivity.

Figure 3 shows a sketch of such a sensor. The size of the chip used for the experiments was 8 mm x 3 mm x 0.35 mm. LN was chosen as substrate for the sensor element because of the high coupling coefficient that provides a high freedom in sensor design and linear sensitivity to strain (Bruckner, 2013).

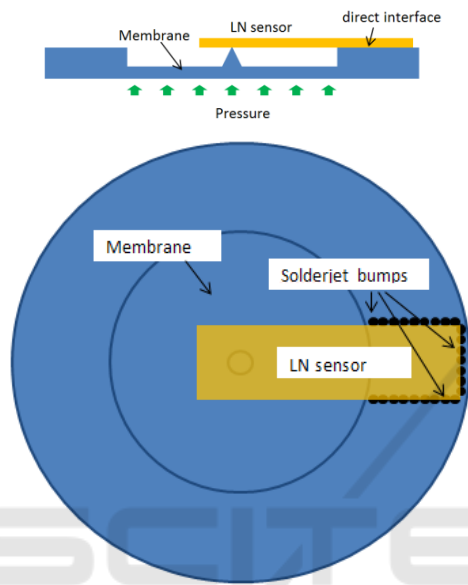


Figure 3: Schematics for a pressure sensor with thin membrane and chip as cantilever.

### 3 ASSEMBLY EXPERIMENTAL DETAILS

For this study, the solderjet bumping laser energy parameters (represented by varying the laser current (mA) and the laser pulse (ms)) were tuned to provide the optimal wetting and strength of  $\text{Au}_{80}\text{Sn}_{20}$  100  $\mu\text{m}$  diameter spherical solder-bumps on a metalized LN substrate.  $\text{Au}_{80}\text{Sn}_{20}$  was selected due to its melting temperature, low enough not to damage the crystal during soldering alloy reflow, but high enough to resist temperatures close to 300  $^{\circ}\text{C}$  required for the final device application. The goal was to successfully assemble a LN crystal to a stainless steel baseplate. The study was done by following a design of experiments (DoE) using input factors, the laser current (mA) and laser pulse (ms), to study the material responses: i) damage to the material, ii) correct wetting provided by a correct bump melting diameter, and iii) force needed to shear the bumps.

An important factor in this assessment was to avoid damage to the LN substrate. A common problem with use of LN is its high tendency to receive photorefractive damage, which results in a change in inhomogeneity of the refractive index of the material (Levinstein, 1967). Another important factor is the difference of strength and wetting of  $\text{Au}_{80}\text{Sn}_{20}$  solder on both LN and stainless steel by applying bumps using the same current and pulse energy, which is attributed to their respective thermo-mechanical characteristics. The relevant material characteristics of the substrate material, the LN and the selected alloy are listed in Table 1.

Table 1: Thermo-mechanical properties of used materials.

	Lithium-Niobate	Stainless Steel	$\text{Au}_{80}\text{Sn}_{20}$
Density (g/cm <sup>3</sup> )	4.64	8	14.7
Young's Modulus (GPa)	170	195	68
Thermal Conductivity (W/mK)	4.4	16.2	57,0
Melting Temp ( $^{\circ}\text{C}$ )	--	--	280

#### 3.1 Initial Tests

Preliminary tests were performed to determine the maximum and minimum laser energy parameters. The maximum energy was determined when the energy was the highest possible without damaging the substrate, while the minimum was determined when the energy was lowest while still allowing flow of the solder bump through the solderjet bumping jet capillary (Figure 1). After preliminary tests were done to find the maximum and minimum energy parameters, a DOE was designed by using twenty-six different laser energy points represented by their laser current (mA) and laser pulse (ms).

The initial created damage was analyzed through visual inspection, rating the damage on a scale of 1 to 4. (Figure 4).

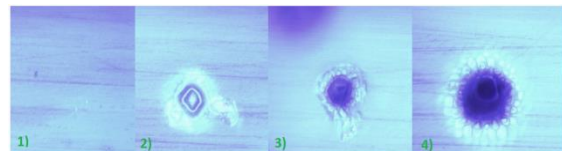


Figure 4: Example of examined damage. (1) No presence of damage; (2) material abrasion; (3) crack; (4) major crack.

The diameter and shear strength results are displayed graphically with a contour map on Figure 5. In Figure 5, the damage on the LN substrate is shown in red numbers at each point on the map (Upper image).

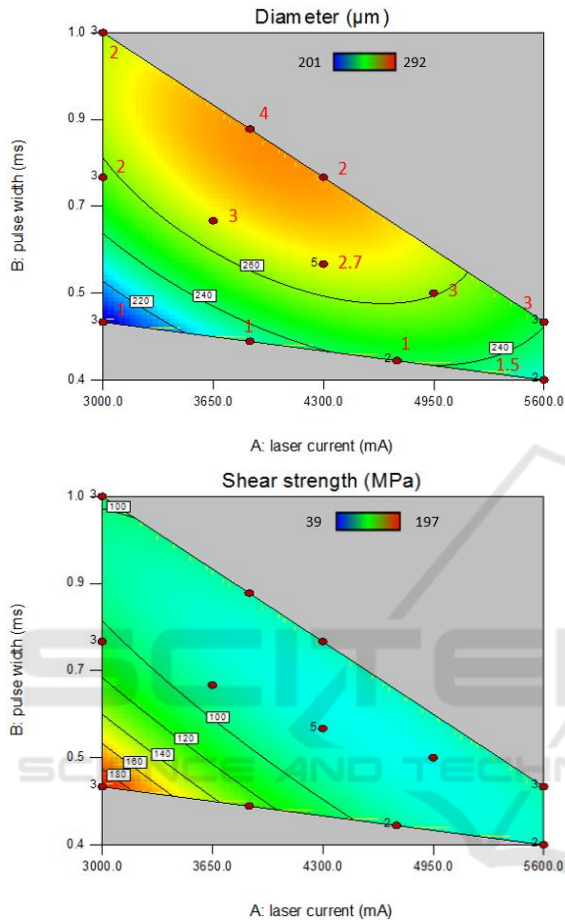


Figure 5: Results of DoE. Upper image, bump diameter and in red numbers damage to assess correct wettability. Image below, bump shear strength results.

The ideal diameter of solder bump after reflow should be approximately 175% to 200% of the original solder sphere (Mäusezahl, 2016); for the case of 100 µm it should be about 175 to 200 µm. As can be seen in Figure 5, there are some results that have an approximate diameter size of 200 µm, in particular bumps with laser energy parameters of 3000 mA/0.5 ms, 3866 mA/0.5 ms, and 4733 mA/0.4 ms. These samples also showed no damage and good resulting shear strength.

The tensile strength of Au<sub>80</sub>Sn<sub>20</sub> is 275 MPa (Indium Corp., 2013) and typically shear strength within metals is estimated to be 50% to 60% of the ultimate tensile strength (Callister, 2013). For our case, this results in an estimation of 137.8 to

165 MPa. In Figure 5, it can be seen that in cases with very high laser energy, shear strength was much below this estimation, however at lower energies shear strength was still slightly above this estimation. Figure 6 shows an example of a sheared solder bumps using low energy (left) and high energy (right). A possible reason for the weakening of Au<sub>80</sub>Sn<sub>20</sub>, is the formation of AuSn<sub>4</sub>, a common occurrence when soldering with tin and gold material. This compound is known to weaken the material and the joint. Higher energy may allow easier formation of AuSn<sub>4</sub> (Hare, 2010).

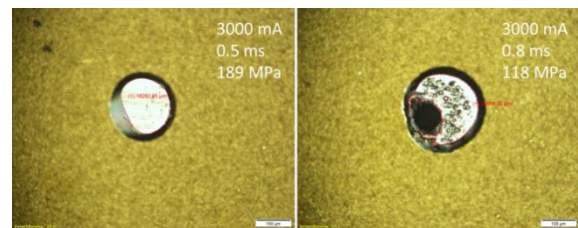


Figure 6: Shear test examples performed using 100 µm AuSn bumps. Left, low energy similar to 8.9 mJ by using a solderjet bumping settings of 3000 mA and 0.5 ms. Right, high energy similar to 15 mJ by using a solderjet bumping settings of 3000 mA and 0.8 ms.

These energies were also tested on stainless steel, the base metal in which the LN is to be bonded to. Examples of the results are shown in Figure 7. The shear strength and wetting diameter values for these samples are shown to be much higher than those that were soldered on the layered LN substrate. The reason for this may be due to the significantly different thermal conductivity in LN and stainless steel. Stainless steel's higher thermal conductivity allows for a larger spread of heat within the metal during the period that the laser contacts the surface. This larger heated area allows for easier wetting of Au<sub>80</sub>Sn<sub>20</sub> solder. In LN, its low conductivity means that heat will remain concentrated in a small area, meaning that this area may achieve a higher temperature than that of stainless steel, during laser contact. As we have seen from the design of experiments, higher laser energy, which correlates to higher temperature, results in lower shear strength. This may explain the reason why LN solder samples show lower wetting diameters and lower shear strength. The optimized laser energy was finally obtained by using the laser values of 3000 mA and 0.5 ms (representing and approximate energy of 8.9 mJ).

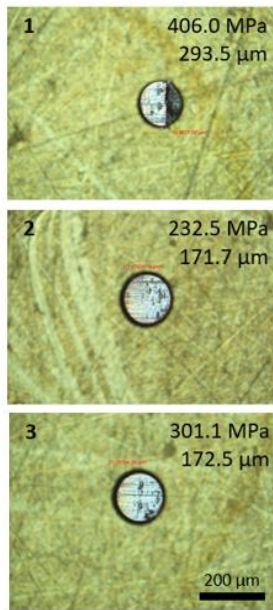


Figure 7: Similar selected energy tests on stainless steel. (1) 3000 mA/0.5 ms showed a bumped diameter of 293.5  $\mu\text{m}$  and a shear force of 406 MPa. (2) 3866 mA/0.5 ms showed a bumped diameter of 171.7  $\mu\text{m}$  and a shear force of 235 MPa. (3) 4733 mA/0.4 ms showed a bumped diameter of 172.5  $\mu\text{m}$  and a shear force of 301 MPa.

The final selected laser parameters (3000 mA and 0.5 ms) were used to create a prototype LN and stainless steel assembly which was later tested for its strength and durability.

### 3.2 Assembly Procedure

Pac Tech's Solder Ball Bumper SB2-Jet was used to solder 100  $\mu\text{m}$  AuSn bumps onto the surface of metalized LN substrate and stainless steel base.

Using the selected optimal laser energy of 8.9 mJ represented by using and 3000 mA and 0.5 ms, LN samples were soldered to stainless steel with the following methods. The LN samples were temporarily secured to stainless steel to later be rotated by 45°, resulting in the desired jointing edges facing up toward the solderjet bumping capillary (Figure 8(a)). Two methods were used to create a joint between the LN and stainless steel. In the first method, a rectangular pattern of four by ten bumps was placed in four locations along each long edge of the LN sample. These were placed in a way that half the solder bump pattern bonded with the LN and the other half bonded with the stainless steel (Figure 8(b)). The second method was similar to the first, except that the bump pattern was only placed in three locations per side. This pattern was also overlaid,

with one on top of the other (Figure 8 (c)) to secure the bond between bumps.

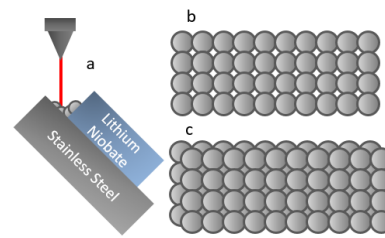


Figure 8: Schematic drawing of different soldering approaches of 100  $\mu\text{m}$  solder bumps application. (a) Schematic of the process with the laser reflow being applied onto the bumps. (b) First described method. (c) Second described method.

Following this method, several prototypes were assembled as described (Figure 9).

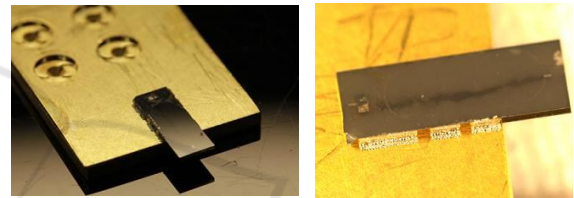


Figure 9: Finally assembled samples.

## 4 ENVIRONMENTAL TESTING

### 4.1 Push Tests

With the selected laser energy, the LN was secured onto stainless steel using the two methods described in the Assembly Procedure section (Figure 8 and Figure 9). This was then subject to a push test. The graphical results of the push test for methods 1 and 2 are shown in Figure 10. The first method showed a maximum strength of 18.1 N. The graph of the second method shows a spike occurring at 18.8 N, and then suddenly dropping to zero, then rising again and remaining steady at about 3 N. The initial spike represents the force in which the LN broke from the soldered joint, and the drop represents a sudden slip after failure. The steady 3 N force indicates the LN continued to slide between the solder joints. Comparing the results of these two methods, it seems that the second method is slightly better than the first with a higher failure force. The disadvantage of this method however is that more time and solder alloy is required. Considering this and the small difference of 0.7 N force observed between the two methods, the

first assembly method was selected as the most optimal.

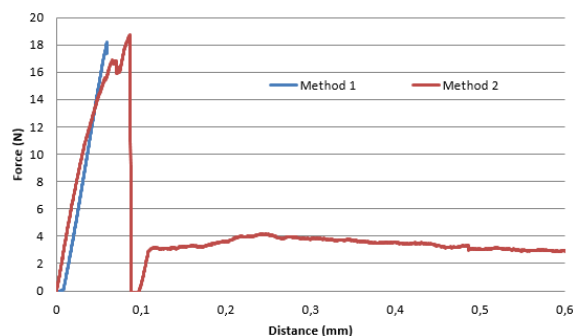


Figure 10: The graphical results of the push test for methods 1 and 2. The graphic represents the moving distance of the Push tests machine (Zwick Roell Z020) and the derivate force applied onto the LN assembled crystal.

## 4.2 Thermal Tests

Thermal annealing tests were performed on four samples at 300 °C to prove the devices operation requirements. First the temperature was slowly increased from room temperature at a rate of 100 °C/h, to finally be kept at a constant 300 °C for 12 h. Afterwards the samples were optically inspected to check for cracks of the LN chips induced by thermal stress. As all samples passed the test successfully they were exposed to a strong temperature gradient by putting the devices from room temperature directly into a hot environment at 300 °C and out again. All devices could withstand three cycles without cracks. Further test are planned with larger number of samples applying different temperatures.

## 5 CONCLUSIONS

Both, the optimal shear strength and wetting parameters to assemble the lithiumniobate crystal to a stainless steel sub-mount were shown to be at 3000 mA and 0.5 ms. The general pattern is that lower laser energies results in higher shear strength and smaller wetting diameters for the solder bumps. Soldering Au<sub>80</sub>Sn<sub>20</sub> to stainless steel results in larger wetting diameters and higher shear strength than when soldered to lithiumniobate, likely due to the higher thermal conductivity of stainless steel.

The two assembly methods produced remarkably similar results in their strength, however considering that the second method uses more material and time to be performed, the optimal method is chosen to be

the first one. The final selected method showed to be capable of handling the required strength demands imposed by the final device application.

Moreover, other author's publications focused on the study of the birefringence effects produced by the described soldering procedure showed how solderjet bumping process can assemble optical components with just a residual stress without affecting the device optical performances (Ribes-Pleguezuelo, 2016; Ribes-Pleguezuelo, 2017). Previous studies and publications make us consider that the same residual effect will not alter the device functionality for the present assembled devices.

## ACKNOWLEDGEMENTS

The authors want to acknowledge other members of the Fraunhofer IOF for their support, especially to Marcel Hornaff for the provided help with the DOE. To the Deutscher Akademischer Austauschdienst (DAAD).

This project is partly supported within the COMET – Competence Centers for Excellent Technologies - Program by BMVIT, BMWFJ and the Province of Carinthia.

## REFERENCES

- Banse, H., Beckert, E., Eberhardt, R., Stöckl, W., Vogel, J., 2005. Laser Beam Soldering – a New Assembly Technology for Microoptical Systems. In *Microsystems Technologies 11*, pp. 186-193.
- Bardong, J., Binder, A., Toskov, S., Miskovic, G., and Radosavljevic, G., 2016. Investigation of low-temperature cofired ceramics packages for high-temperature SAW sensors. In *J. Sens. Sens. Syst.*, 5, p 85–93.
- Beckert, E., Oppert, T., Azdasht, G., Zakel, E., Burkhardt, T., Hornaff, M., Kamm, A., Scheidig, I., Eberhardt, R., Tünnermann, A., Buchmann, F., 2009. Solder Jetting - A Versatile Packaging and Assembly Technology for Hybrid Photonics and Optoelectronic Systems. In *IMAPS 42nd International Symposium on Microelectronics, Proceedings, Vo. 42*, pp. 406-412.
- Bruckner, G., Schicker, J., Schlumpf, P., 2013. Stress sensitivity of SAW Rayleigh waves on Lithiumniobate and its application in pressure sensor design. *Proceedings IEEE International Ultrasonics Symposium (IUS), Prague*, pp. 2140-2143.
- Bruckner, G., Bardong, J., Binder, A., Nicolay, P., 2017. SAW Delay Lines as Wireless Sensors for Industrial Applications. *Proceedings of the VIII ECCOMAS Thematic Conference on Smart Structures and Materials, SMART 2017, Madrid*, pp. 1433-1442.

- Callister, W. D., Rethwisch D. G., 2013. *Materials Science and Engineering: an Introduction*. Wiley, New Jersey, 9<sup>th</sup> edition.
- Hare, E., 2010. *Gold Embrittlement of Solder Joints*. In SEM Lab, INC. [www.semlab.com](http://www.semlab.com)
- Indium Corporation, 2013. Gold-Tin: The Unique Eutectic Solder Alloy. In [www.documents.indium.com/qdynamo/download.php?docid=2103](http://www.documents.indium.com/qdynamo/download.php?docid=2103).
- Levinstein, H. J., Ballman, A. A., Denton, R. T., Ashkin, A., Dziedzic, J.M., 1967. Optically Induced refractive index inhomogeneities in LiNbO<sub>3</sub> and LiTaO<sub>3</sub>. In *Applied Physics Letters*, vol. 9, no. 1, 1966, pp. 72–74; doi:10.1063/1.1754607.
- Mäusezahl, M., Hornaff, M., Burkhardt, T., Beckert, E., 2016. Mechanical Properties of Laser-Jetted SAC305 Solder on Coated Optical Surfaces. In *Physics Procedia*, vol. 83, 2016, pp. 532–539; doi:10.1016/j.phpro.2016.08.055.
- Reindl, L., Scholl, G., Ostertag, T., Scherr, H., Wolff, U., Schmidt, F., 1998, Theory and Application of Passive SAW Radio Transponders as Sensors. *IEEE Trans. Ultrason. Ferroelectr. Freq. Control* 45 (5), pp.1281-1292.
- Ribes-Pleguezuelo, P., Koechlin, C., Hornaff, M., Kamm, A., Beckert, E., Fiault, G., Eberhardt, R., Tünnermann, A., 2016. High-precision optomechanical lens system for space applications assembled by a local soldering technique. In *Opt. Eng.* 55(6), 065101 (2016); doi: 10.1117/1.OE.55.6.065101.
- Ribes-Pleguezuelo, P., Zhang, Z., Beckert, E., Eberhardt, R., Wyrowski, F., Tünnermann, A., 2017. Method to simulate and analyse induced stresses for laser crystal packaging technologies. In *Optics Express* Vol. 25, No.6; doi:10.1364/OE.25.005927
- Roshanghias, A., Bruckner, G., Binder, A., 2017. High temperature MEMS packages: die-attach solutions for LiNbO<sub>3</sub> under low bonding pressures. In *J Mater Sci: Mater Electron*, DOI 10.1007/s10854-017-6605-3